Nanoscale Imaging of Neutral Atoms with a Pulsed Magnetic Lens

Rodrigo Castillo-Garza,* Jamie Gardner, Sagi Zisman, and Mark G. Raizen

Center for Nonlinear Dynamics and Department of Physics, The University of Texas at Austin, Austin, Texas 78712, United States

ABSTRACT We present a scheme for imaging of neutral atoms to the nanoscale with a pulsed magnetic lens and show its viability through numerical calculations. This scheme achieves focal lengths on the order of several centimeters and focal spots of less than 10 nm. With these results, it is possible to create sub-10 nm structures on surfaces in a parallel and time-efficient manner. When used with metastable noble gas atoms, and in combination with electron spectroscopy, this scheme can create a chemically sensitive microscope which can probe surfaces on the nanometer scale.

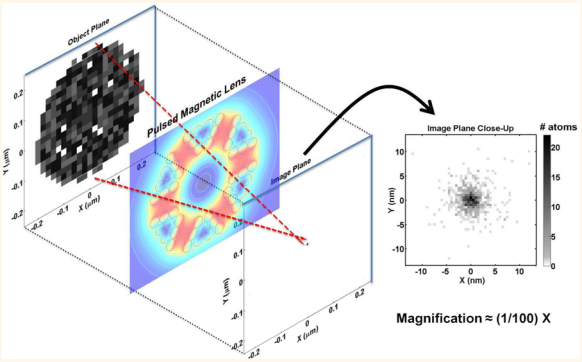

KEYWORDS: nanolithography · pulsed magnetic lens · nanocharacterization · atom microscope · sub-10 nm · tapered hexapole · chemically sensitive probe

Great advances in nanolithography and nanofabrication over the years have been constantly pushing the limits of resolution. Despite these impressive results, it is clear that in order to reach the few nanometer level, a new approach is required. Parallel, top-down approaches based on photolithography are limited by the wavelength of the light that is used for these processes.

State-of-the-art technology can now achieve a feature size of 20−100 nm.[1,2] While other top-down approaches based on electron-beam lithography can achieve nanometer scale structures, they are limited by the thickness of the resist and are inherently very slow.[3,4] Alternate methods that rely on bottom-up techniques are based on molecular self-assembly.[5] These can achieve nanometer scale structures, but they are currently limited by random thermal processes.[6] The possibility of using neutral atoms in a beam to reach the nanometer scale resolution stimulated a great deal of work, starting over 20 years ago.[7−11] This field, known as atom lithography, mainly utilized standing waves of light to focus the atoms.[7,9] While the basic method was successful, it was limited to parallel lines and a few simple specific arrays[12] due to the periodic nature of a standing wave of light. The resolution of atom lithography was also limited by severe aberrations of the standing wave, a fundamental problem that has stopped further progress.[12]

An alternative approach is to use the magnetic moment of an atom, which is a nearly universal property of most elements in the periodic table. In previous work, permanent magnets have been used to focus atoms.[10,13] The refractive power of these magnetic lenses is a function of the gradient of the magnetic field and the magnetic moment to mass ratio of the atom. The method has been limited so far by the low magnetic field gradients available, which result in a large focal length, as well as by the fringe fields that the atoms experience as they enter and leave the magnets. Clark *et al.*[14] recently proposed a parallel method to achieve focal spots with dimensions of sub-10 nm; however, that method does not enable true imaging and hence has limited applicability.

Here we propose an efficient method to control the structure of materials at the nanometer scale. In this method, a small bunch of fast and cold atoms produced with a pulsed supersonic source is divided into several bunches of atoms with a perforated

* Address correspondence to rcastillogarza@chaos.utexas.edu.

Received for review February 21, 2013 and accepted April 1, 2013.

Published online 10.1021/nn400896y

© XXXX American Chemical Society

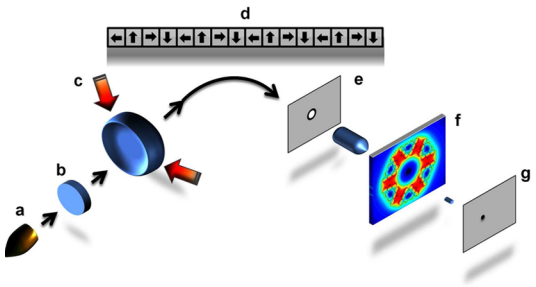

Figure 1. Schematic diagram of the proposed experimental setup. (a) Even-Lavie pulsed supersonic nozzle with a high-voltage pulsed discharge. (b) Initial spatial extent of the bullet of atoms. (c) Brightening of the beam, reduction of beam's dispersion, and optical tagging of the bullet. (d) Magnetic mirror. (e) Transmission mask with a circular aperture (the object plane). (f) Pulsed magnetic lens. (g) Image plane. The lines represent the trajectories of paramagnetic atoms. The angle between the supersonic beam and the mirror selects the magnetic species that enter the magnetic lens. In this configuration, atoms of a particular low-field-seeking state are selected and the rest of them are rejected.

pattern on a transmission mask. The pattern is then imaged to a much smaller size by a pulsed magnetic lens. A schematic diagram of an experimental setup for this method is shown in Figure 1. It contains an Even-Lavie pulsed supersonic source (Figure 1a), a magnetic mirror (Figure 1d) to select the magnetic state of the atoms that enter the lens, and a pulsed magnetic lens (Figure 1f). Due to the geometry and extent of the lens, this method can enable parallel nanofabrication of structures. In addition, this lens is aberration-corrected, and it is effective on all atoms that are paramagnetic, which encompass most elements in the periodic table.

The choice of a high-flux pulsed supersonic source (Figure 1a) is a critical starting point for this work, as it produces a fast and a highly monoenergetic beam, $\Delta v_{\|}/v_{\|} \sim 0.01$, with an intensity of 10^{24} atoms/(sr s).[15] It can produce pulse widths as low as 10 μs at a frequency of up to 1 kHz.[15] Furthermore, this source can be used in conjunction with seeding techniques, such as laser ablation, to produce a supersonic beam of any element in the periodic table and of many molecules.[16] In the important case of noble gas atoms that are nonmagnetic in their ground state, such as helium or neon, they can be excited to a long-lived metastable state by employing a pulsed discharge near the nozzle[17] (Figure 1a). Metastable atoms are particularly useful, as will be described below.

Once these atoms exit the source, they form a bullet (Figure 1b) that will be optically manipulated to enhance the image contrast and to allow the lens to correct for aberrations (Figure 1c). For the former, we will increase the beam brightness with an optical 2D molasses setup, as this technique has been successful in achieving high brightness values.[18,19] For the latter, we will reduce the longitudinal velocity spread ($\Delta v_{\|}$) in the bullet's frame of reference and optically tag the bullet (Figure 1c) as it comes out of the source. To reduce $\Delta v_{\|}$, we plan to laser cool the atoms in the longitudinal direction but without changing their initial average velocity ($v_{\|}$). To tag the bullet, we would optically pump a thin (100 μm) slice of the bullet to a certain magnetic state and pump the rest to a different magnetic state.

The desired magnetic state of the atoms will be selected with a magnetic mirror in a planar Halbach configuration.[20,21] This mirror consists of a collection of constant amplitude permanent magnets, each arranged according to the direction of their individual magnetization. Each magnet's magnetization is rotated 90° with respect to its nearest neighbors and follows a sense of rotation (Figure 1d). This periodic configuration produces, on one side only, an inhomogeneous magnetic field (B) that decays exponentially in the normal direction to the mirror. This field interacts with the magnetic dipole of the atoms in the beam. Their interaction energy is

$$U = m_F g_F \mu_B B \qquad (1)$$

where m_F is the magnetic quantum number of the particle, g_F is the Landé g-factor and μ_B is the Bohr magneton. Low-field-seeking atoms with $m_F g_F > 0$ are pushed away from the mirror, while atoms with $m_F g_F < 0$ are attracted to it. The mirror is positioned at an angle with respect to the beam direction such that the thin slice of the bullet is reflected and directed toward the transmission mask (Figure 1e). For instance, using commercial neodymium magnets (remanence $\sim$ 1.3 T) in the mirror, this angle is $\sim$2.5° for metastable neon at 300 K in the 3^3P_2 $m_F = +2$ state. This selection method allows for the focal plane to be out of sight of the source and for the beam divergence to be unaltered. More importantly, as will be shown below, this selection of a slice allows the lens to correct for aberrations.

Since supersonic sources produce fast atoms, a lens with high refractive power is required to achieve practical focal lengths, on the order of centimeters. Current permanent magnet technology has not yet offered a viable solution.[22] Instead, we propose using a lens based on a pulsed, coreless electromagnet (Figure 2). An electromagnet generates an inhomogeneous magnetic field and provides complete control of the field's magnitude through the modification of its current. Its refractive power is a function of the same parameters as that of the permanent magnets, as the interaction energy between a magnetic dipole of an atom and the field is that of eq 1. To achieve the desired refractive power, the electromagnet we are proposing has to generate a magnetic field gradient of 1−2 T/mm. A practically advantageous method to accomplish this is using a pulsed electromagnet with small dimensions, $\sim$O(mm). This is a common technique that has been successfully used to generate the magnetic field gradients we require.[15]

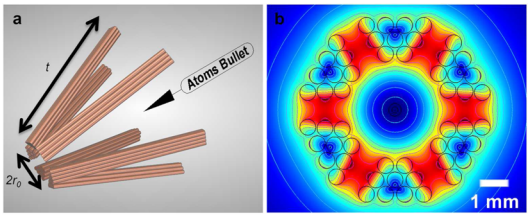

Figure 2. Electromagnetic Lens. (a) Tapered hexapole configuration. Wire configuration tapers off toward the center of an imaginary hexagon as particles traverse through it, where $t^2 = (r_i - r_0)^2 + L_0^2$. (b) Cross section of the magnetic lens while switched on. Magnetic field is calculated with finite element methods. The color scale represents the magnitude of the magnetic field: The field in the light-blue zones is greater than the field in the dark-blue zones, the latter being the lowest field. The thin light-blue contour lines show where the magnetic field is constant. The black line circles surrounding the hexapole field represent the wires.

The electromagnetic lens we are proposing is aberration-corrected. It consists of six wire bundles along the longitudinal direction of the atomic beam, each at the vertex of an imaginary hexagon. The bundles are slanted, while keeping the hexapole cross section. They linearly decrease their distance to the center of the hexagon as seen by the particles traversing this wire configuration. Figure 2a shows a diagram of the tapered electromagnetic lens. The configuration of the electric current running through the bundles is chosen to produce a hexapole field. Figure 2b depicts a schematic diagram of the cross section of this magnetic field and the wire bundle configuration.

Through the magnetic interaction energy of eq 1, a hexapole field exerts on each atom a radial force that is proportional to its distance from the center. Tapering off the hexapole results in a radial force, F_r, and a longitudinal force, F_z. Both forces depend on the distance of the atoms from the center and their longitudinal position in the lens:

$$F_r = -\{2\mu_B g_F |m_F|\} \times \left\{1 - \left(\frac{r_i - r_0}{r_0 L_0}\right)(z - L_0)\right\}^{-2} \times B_0 \frac{r}{r_0^2} \quad (2)$$

and

$$F_z = -\{2\mu_B g_F |m_F|\} \times \left\{\frac{r_i - r_0}{r_0 L_0}\right\} \times \left\{1 - \left(\frac{r_i - r_0}{r_0 L_0}\right)(z - L_0)\right\}^{-3} \times B_0 \frac{r^2}{r_0^2} \quad (3)$$

$L_0 \sim \langle v_\parallel \rangle \Delta t$ is the effective lens width. Along this distance, the atoms interact with the tapered hexapole for a time Δt, which is the electromagnet pulsing time. B_0 is the magnetic field at $r = r_0$, the smallest inner radius of the lens, and r_i is the largest inner radius. This geometry results in the following tapering angle (α):

$$\alpha = \tan^{-1}\left(\frac{r_0 - r_i}{L_0}\right) \quad (4)$$

The force in eq 2 can focus a beam of low-field-seeking particles correcting for chromatic aberration and the effects of the spatial extent of the bullet as it exits the source. For this to be successful, the longitudinal position of the atoms in the bullet when inside the lens has to be correlated with their initial longitudinal velocity. This allows for F_r to be larger for faster atoms than for slower atoms, therefore reducing the lens' focal length for faster atoms and increasing it for the slower ones. We achieve this correlation through the selection, as described above, of a thin slice of the bullet of atoms at the source, where their longitudinal velocity and position are uncorrelated. If the hexapole's tapering angle is correctly selected, the focal length associated with each atom will be forced to converge to the same value, therefore effectively reducing chromatic aberration and aberration effects due to the spatial extent of the bullet at the source.

The longitudinal force of eq 3 resembles spherical aberration from optical lenses, as it is stronger near the edges of the lens. Its effects are minimal in our setup since the atomic beam width in the lens is smaller than the lens aperture by at least 1 mm. Furthermore, the absolute value of this force is much smaller than the radial force of eq 2 for the effective part of the lens (L_0), allowing us to neglect its effects. Its effects were confirmed in our numerical calculations.

Additional aberrations arise due to deviations from the hexapole field. This occurs close to the wire bundles due to its geometry and due to dispersion forces. Their effects are minimized by keeping the atomic beam width small and far from the bundles when inside the lens. An additional source of aberration is due to the finite size of the lens in the longitudinal axis. The ends of the lens produce fringe fields that deviate from the magnetic field of a hexapole. We minimized the effect of these fields on the atom trajectories using the pulsing feature of the electromagnet. That is, the timing of the current pulse generating the magnetic field is synchronized with the pulsed source so that only a hexapole-like field interacts with the atomic beam bunch.

To show the performance of this imaging method, we use finite element analysis and numerical integration to simulate the path of metastable helium (He*) atoms as they traverse the elements of this imaging method. We evaluate the performance of this method in terms of the image that the magnetic lens produces. For this simulation, we use a pulsed beam of He* in the 2^3S_1 state and with $m_F = +1$. The spatial extent of the bullet's thin slice is 70 μm (FWHM) which, as was described above, would have been selected when combining optical tagging (Figure 1c) and a planar Halbach array (Figure 1d). The source size for this beam is 600 μm, its temperature is 20 K, and it is 1.4 m away from the transmission mask. The source produces a pulsed beam of He* atoms with an average longitudinal

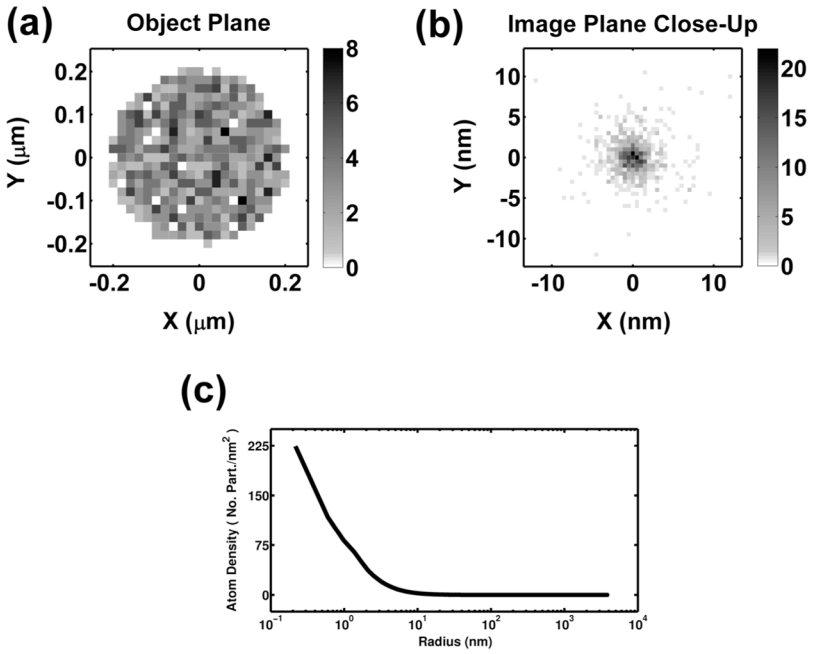

Figure 3. Imaging a beam of atoms through a 400 nm circular aperture. Two-dimensional histograms of the position of the atoms on the (a) object plane and a (b) close-up of the center of the image plane. The gray scale bars indicate the color code for the number of atoms. (c) Density of He* atoms as a function of their radial position on the image plane.

speed of $v_{\|} = 455.77$ m/s and a relative beam dispersion of $\Delta v_{\|}/v_{\|} \sim 2e^{-5}$. The latter is assuming that we have laser-cooled the He* atoms from the beam in the longitudinal direction and that they have reached the recoil cooling limit. The atomic beam is coaxial with the perforated mask and the axis of the tapered hexapole lens. The distance between the mask and the lens (analogous to the object distance in optics) is 1.75 m. Once the beam is in the lens, the magnetic field is switched on for 16 μs. The lens dimensions are $r_0 =$ 1.5 mm and $r_i = 2.155$ mm. No fringe fields are considered, as the atomic beam pulse is mostly inside the lens. With a current pulse of $I = 900$ A, the lens produces a magnetic field gradient of ~1 T/mm and results in a focal length of $f \sim 15.4$ mm, as measured from the beginning of the lens.

RESULTS AND DISCUSSION

Two image planes are examined: In the first case, we show the image produced by 1000 He* atoms traversing a 400 nm circular aperture on the mask. In the second case, we show the image produced by 1000 He* atoms traversing through an array of four 400 nm circular apertures. In the first case, the aperture is centered with the hexapole field center and an image is produced at ~1.78 m away from the mask. This corresponds to an image distance of ~15.5 mm, as measured from the beginning of the lens. Figure 3b shows the image plane and Figure 3a the object plane. This former figure shows the position of the He* atoms at the image plane in a 2D histogram, where each bin has dimensions of 0.5 nm × 0.5 nm. The gray scale bars indicate the color code for the number of atoms. While the atoms are spread on the image plane, most bins contain either zero or a few He* atoms. This is not the case for the bins at the center of the image, where a dark spot of about 4 nm × 4 nm contains most of the He* atoms from the beam bunch. These statements are more evident in Figure 3c, where the density of atoms is plotted as a function of the radial position of the atoms from the center of the image. Note that the effective demagnification factor of the lens is 100×, which is in agreement with the image distance to object distance ratio used in light optics.

The diffraction limit of this lens setup is about 6 nm. However, the atom spot size is not diffraction-limited. Shorter focal lengths can be attained with higher currents through the lens and larger numerical apertures. Particularly for this setup, the latter can be achieved by reducing the initial beam collimation and allowing a larger size beam to enter the lens. A minimum diffraction limit of about 1 nm could be achieved.

In the second case we simulated, imaging four circular apertures on the transmission mask, we show the parallel capability of the imaging method described in this article. All of the apertures on the mask (the object plane) have a 400 nm diameter and a pitch of 20 μm. Furthermore, passing through each aperture, there are a total of 250 He* atoms. In Figure 4, we show 2D histograms of the position of the atoms on the (a) object plane and on a (b) close-up of the image plane. Figure 4c shows a closer look at one of the features in Figure 4b. This feature is indicated by a black arrow in

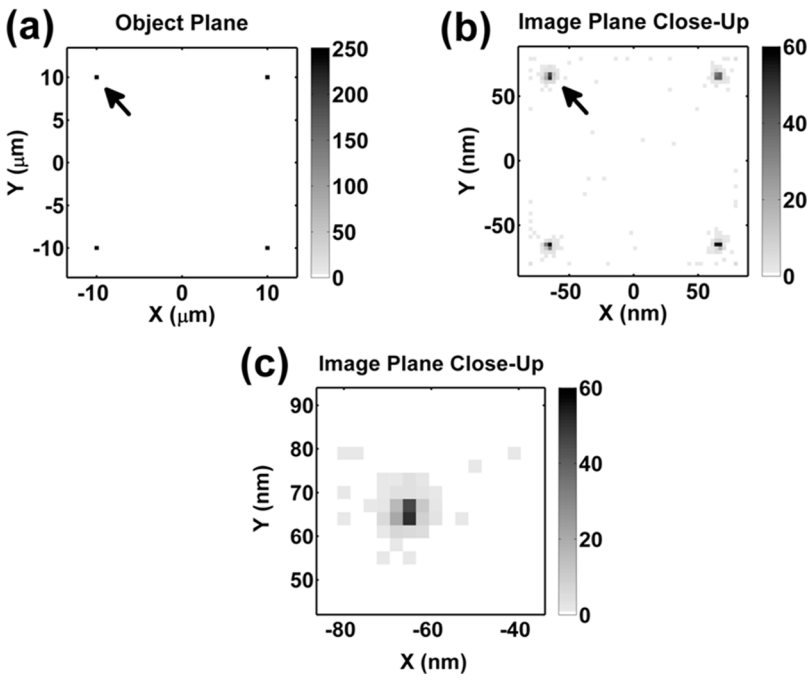

Figure 4. Parallel capability of the imaging method presented. Two-dimensional histograms of the position of the atoms (a) on the object plane, (b) on a close-up of the image plane, and (c) on a zoom-in of one of the features on the image plane (marked with an arrow in panels a,b). The (a) object plane has four black 500 nm × 500 nm bins that represent the number of atoms traversing through the 400 nm apertures on the transmission mask. The gray scale bars indicate the color code for the number of atoms.

Figure 4a,b. Similarly to Figure 3, the image plane of Figure 4b has bins with few He* atoms and bins with large numbers of them, except that they are in separate and in specific sites. These sites have a pitch of about 200 nm, and each of them extends for about 15 nm × 15 nm. Note that in this figure and in Figure 4c the bin dimensions are 3 nm × 3 nm, and most of the particles in each of these sites are contained in an area of 6 nm × 6 nm (Figure 4c). In fact, Figure 4c shows that more than 50% of the particles going through each aperture are in this area. As was found in the first case, the lens demagnification factor is about 100×.

Considering the parameters used in the simulation of the beam passing through a single 400 nm aperture and the techniques we mentioned to prepare the beam, we have estimated that ~10−100 He* atoms will go through the aperture with each nozzle pulse. While this value may be sufficient for our immediate purposes, this value is not yet limited. It can be increased by at least 100 if sub-Doppler techniques of laser cooling are used to increase the beam's brightness. Alternatively, we can increase the contrast of the image by increasing the pulse frequency of the nozzle and magnet lens.

Incorporating laser cooling and optical pumping techniques to this imaging method reduces the number of atomic species that can be utilized. Nevertheless, their combination can be successfully used for patterning, as was the case for previous focusing schemes using molecular resists based on self-assembled monolayers.[23] In contrast with those schemes, the method described here will be able to pattern surfaces with higher spatial resolution, in less time, and with reduced complexity. The extension to other atomic species requires a new brightening method other than laser cooling, as proposed by M. G. Raizen and E. Narevicius (personal communications).

CONCLUSIONS

The method we are proposing is not only useful for parallel manufacturing of sub-10 nm structures, but it can also be used as an atom microscope. In analogy to electron-beam lithography and a scanning electron microscope, a focused beam of metastable atoms can be used to pattern as well as to probe a substrate. In this method, metastable atoms have thermal kinetic energies of ~O(10^{-2} eV) and carry an excitation energy with respect to their ground state of ~ O(10^{1} eV). This latter energy is released when in contact or close to contact with a surface. When metastable atoms are used for patterning, this energy breaks the molecular bonds of a resist. When they are used to probe surfaces, this energy releases electrons from a substrate. In fact, electron spectroscopy of surfaces using metastable atoms has been a powerful technique in surface science,[24,25] especially because it probes the outermost layer of a surface without inflicting significant damage, as compared to scanning electron microscopy, and has a spatial resolution of approximately micrometers.[26] Since the kinetic energy of the released

electrons depends on the work function and the electronic properties of the bombarded material, the combination of this technique with a focused beam of metastable atoms can be a chemically sensitive nanoprobe. This technique can be used to probe and understand materials in the forefront of science and technology, such as high-T_c superconductors, doped semiconductors, and topological insulators, in which desirable electronic properties may rely on the chemical composition at the nanoscale.[27−29]

METHODS

We use finite element analysis to obtain the magnetic field in the lens and numerical integration to simulate the trajectories of He* atoms as they traverse the elements of this imaging scheme. The parameters used for this simulation can be found above.

Conflict of Interest: The authors declare no competing financial interest.

Acknowledgment. We are pleased to acknowledge Bruce Klappauf and Edvardas Narevicius for helpful discussions and the careful reading of this manuscript. M.G.R. acknowledges support from the Sid W. Richardson Foundation and the R. A. Welch Foundation.

Note Added after ASAP Publication. This paper was published on the Web on April 9, 2013. A change was made to a value in the last paragraph of the first section. The revised version was reposted on April 11, 2013.

REFERENCES AND NOTES

1. Gates, B. D.; Xu, Q.; Stewart, M.; Ryan, D.; Willson, C. G.; Whitesides, G. M. New Approaches to Nanofabrication: Molding, Printing, and Other Techniques. *Chem. Rev.* **2005**, *105*, 1171–1196.
2. Pease, R. F.; Chou, S. Y. Lithography and Other Patterning Techniques for Future Electronics. *Proc. IEEE* **2008**, *96*, 248–270.
3. Chou, S. Y.; Krauss, P. R.; Zhang, W.; Guo, L.; Zhuang, L. In *Sub-10 nm Imprint Lithography and Applications*, Papers from the 41st international conference on electron, ion, and photon beam technology and nanofabrication, Dana Point, California, AVS: Dana Point, California, 1997; pp 2897−2904.
4. Wei, C.; Ahmed, H. Fabrication of 5−7 nm Wide Etched Lines in Silicon Using 100 keV Electron-Beam Lithography and Polymethylmethacrylate Resist. *Appl. Phys. Lett.* **1993**, *62*, 1499.
5. Whitesides, G. M.; Mathias, J. P.; Seto, C. T. Molecular Self-Assembly and Nanochemistry: A Chemical Strategy for the Synthesis of Nanostructures. *Science* **1991**, *254*, 1312–1319.
6. Stangl, J.; Holý, V.; Bauer, G. Structural Properties of Self-Organized Semiconductor Nanostructures. *Rev. Mod. Phys.* **2004**, *76*, 725–783.
7. Timp, G.; Behringer, R. E.; Tennant, D. M.; Cunningham, J. E.; Prentiss, M.; Berggren, K. K. Using Light as a Lens for Submicron, Neutral-Atom Lithography. *Phys. Rev. Lett.* **1992**, *69*, 1636–1639.
8. Berggren, K. K.; Bard, A.; Wilbur, J. L.; Gillaspy, J. D.; Helg, A. G.; McClelland, J. J.; Rolston, S. L.; Phillips, W. D.; Prentiss, M.; Whitesides, G. M. Microlithography by Using Neutral Metastable Atoms and Self-Assembled Monolayers. *Science* **1995**, *269*, 1255–1257.
9. McGowan, R. W.; Giltner, D. M.; Lee, S. A. Light Force Cooling, Focusing, and Nanometer-Scale Deposition of Aluminum Atoms. *Opt. Lett.* **1995**, *20*, 2535–2537.
10. Kaenders, W. G.; Lison, F.; Richter, A.; Wynands, R.; Meschede, D. Imaging with an Atomic Beam. *Nature* **1995**, *375*, 214–216.
11. Drodofsky, U.; Stuhler, J.; Schulze, T.; Drewsen, M.; Brezger, B.; Pfau, T.; Mlynek, J. Hexagonal Nanostructures Generated by Light Masks for Neutral Atoms. *Appl. Phys. B: Laser Opt.* **1997**, *65*, 755–759.
12. Meschede, D.; Metcalf, H. Atomic Nanofabrication: Atomic Deposition and Lithography by Laser and Magnetic Forces. *J. Phys. D: Appl. Phys.* **2003**, *36*, R17.
13. Beardmore, J. P.; Palmer, A. J.; Kuiper, K. C.; Sang, R. T. A Hexapole Magnetic Guide for Neutral Atomic Beams. *Rev. Sci. Instrum.* **2009**, *80*, 073105.
14. Clark, R. J.; Mazur, T. R.; Libson, A.; Raizen, M. G. Nanofabrication by Magnetic Focusing of Supersonic Beams. *Appl. Phys. B: Laser Opt.* **2011**, *103*, 547–551.
15. Narevicius, E.; Libson, A.; Parthey, C. G.; Chavez, I.; Narevicius, J.; Even, U.; Raizen, M. G. Stopping Supersonic Beams with a Series of Pulsed Electromagnetic Coils: An Atomic Coilgun. *Phys. Rev. Lett.* **2008**, *100*, 093003.
16. Smalley, R. E. Laser Studies of Metal Cluster Beams. *Laser Chem.* **1983**, *2*, 167–184.
17. Luria, K.; Lavie, N.; Even, U. Dielectric Barrier Discharge Source for Supersonic Beams. *Rev. Sci. Instrum.* **2009**, *80*, 104102-4.
18. Hoogerland, M. D.; Driessen, J. P. J.; Vredenbregt, E. J. D.; Megens, H. J. L.; Schuwer, M. P.; Beijerinck, H. C. W.; van Leeuwen, K. A. H. In *A Factor 1600 Increase in Neutral Atomic Beam Intensity Using Laser Cooling*, Frequency Control Symposium. 48th Proceedings of the 1994 IEEE International Conference, 1−3 Jun 1994; pp 651−654.
19. Rooijakkers, W.; Hogervorst, W.; Vassen, W. An Intense Collimated Beam of Metastable Helium Atoms by Two-Dimensional Laser Cooling. *Opt. Commun.* **1996**, *123*, 321–330.
20. Hinds, E. A.; Hughes, I. G. Magnetic Atom Optics: Mirrors, Guides, Traps, and Chips for Atoms. *J. Phys. D: Appl. Phys.* **1999**, *32*, R119.
21. West, A. D.; Weatherill, K. J.; Hayward, T. J.; Fry, P. W.; Schrefl, T.; Gibbs, M. R. J.; Adams, C. S.; Allwood, D. A.; Hughes, I. G. Realization of the Manipulation of Ultracold Atoms with a Reconfigurable Nanomagnetic System of Domain Walls. *Nano Lett.* **2012**, *12*, 4065–4069.
22. Kaenders, W. G.; Lison, F.; Müller, I.; Richter, A.; Wynands, R.; Meschede, D. Refractive Components for Magnetic Atom Optics. *Phys. Rev. A: At., Mol., Opt. Phys.* **1996**, *54*, 5067–5075.
23. Baldwin, K. Metastable Helium: Atom Optics with Nano-Grenades. *Contemp. Phys.* **2005**, *46*, 105–120.
24. Morgner, H. The Quantitative Characterization of Liquid and Solid Surfaces with Metastable Helium Atoms. *AIP Conf. Proc.* **2000**, *500*, 687–698.
25. Harada, Y.; Masuda, S.; Ozaki, H. Electron Spectroscopy Using Metastable Atoms as Probes for Solid Surfaces. *Chem. Rev.* **1997**, *97*, 1897–1952.
26. Harada, Y.; Yamamoto, S.; Aoki, M.; Masuda, S.; Ichinokawa, T.; Kato, M.; Sakai, Y. Surface Spectroscopy with High Spatial Resolution Using Metastable Atoms. *Nature* **1994**, *372*, 657–659.
27. Billinge, S. J. L.; Levin, I. The Problem with Determining Atomic Structure at the Nanoscale. *Science* **2007**, *316*, 561–565.
28. Dagotto, E. Complexity in Strongly Correlated Electronic Systems. *Science* **2005**, *309*, 257–262.
29. Hasan, M. Z.; Kane, C. L. Colloquium: Topological Insulators. *Rev. Mod. Phys.* **2010**, *82*, 3045–3067.